Available online at www.sciencedirect.com

ScienceDirect

Ceramics International 40 (2014) 4507–4513

CERAMICS INTERNATIONAL

www.elsevier.com/locate/ceramint

Characterization, antibacterial and *in vitro* compatibility of zinc–silver doped hydroxyapatite nanoparticles prepared through microwave synthesis

Nida Iqbal[a], Mohammed Rafiq Abdul Kadir[a,*], Nasrul Humaimi Mahmood[a], Norita Salim[b], Gabriele R.A. Froemming[b], H.R. Balaji[c], Tunku Kamarul[c]

[a]*Medial Implant Technology Group (MEDITEG), Faculty of Biosciences and Medical Engineering, Universiti Teknologi Malaysia (UTM), 81310 UTM Skudai, Johor Bahru, Johor, Malaysia*

[b]*Institute of Medical Molecular Biotechnology (IMMB), Faculty of Medicine, UiTM Campus Sungai Buloh, Selangor, Malaysia*

[c]*Tissue Engineering Group, NOCERAL, Department of Orthopaedic Surgery, Faculty of Medicine, University of Malaya, 50603 Kuala Lumpur, Malaysia*

Received 22 July 2013; accepted 21 August 2013
Available online 5 September 2013

Abstract

We investigated the possibility of enhancing hydroxyapatite (HA) bioactivity by co-substituting it with zinc and silver. Zn–Ag–HA nanoparticles were synthesized by using the microwave-assisted wet precipitation process, and their phase purity, elemental composition, morphology, and particle size were analyzed by X-ray diffraction (XRD), Fourier transform infrared spectroscopy (FTIR), scanning electron microscopy (SEM), and energy dispersive X-ray spectroscopy (EDX). FTIR, XRD, and EDX results showed the characteristic peaks of the Zn–Ag–HA structure, while SEM results demonstrated that the nanoparticles were of spherical shape with a particle size of 70–102 nm. Antibacterial tests of the nanoparticles revealed their antibacterial activity against *Staphylococcus aureus* and *Escherichia coli*. By using simulated body fluid (SBF), an apatite layer formation was observed at 28 days. *In vitro* cell adhesion assay confirmed the cell attachment of normal human osteoblast (NHOst) cells to the disc surface. MTT [(3(4, 5-dimethylthiazol-2-yl)-2, 5 diphenyltetrazolium bromide] assay indicated that the cells were viable, and the cells proliferated faster on the disks than on the control surface due to the presence of metal ions. In conclusion, the novel Zn–Ag–HA nanoparticles were found to be compatible with *in vitro* experiments and having potential antibacterial properties. Therefore these nanoparticles could be a promising candidate for future biomedical applications.

Keywords: Biomaterial; Bioactivity; Orthopedics; Antibacterial agent; Microwave synthesis

1. Introduction

Bacterial contamination, which results in the colonization of biomaterial surface, is a serious post-implantation problem that has dire consequences in surgical and orthopedic practices [1,2]. Despite its low incidence, infection due to *Staphylococcus aureus* or *Escherichia coli* is a common clinical problem that can result in severe morbidity. Open fractures, in particular, involving large segmental bone defects are prone to such infections. This condition increases the risk of infection management of the bone defect and frequently involves the use of artificial bone grafts or bone substitutes [3–5]. Synthetic hydroxyapatite (HA), $[Ca_{10}(PO_4)_6(OH)_2]$, is commonly used in orthopedic applications owing to its biocompatibility and osteoconductive properties [6,7]. It has been reported that incorporation of trace ions such as Ag, Zn, Ti, and Cu into HA structures not only provides crystallinity, but also improves their antimicrobial property [8–10]. Zn is present in all biological tissues, stimulates bone mineralization, and helps in pathological calcification. Bone is the main reservoir of Zn, which accounts for 28% of the total Zn content in the body. In addition, Zn also plays a vital role in the maintenance of membrane structure, function, protein synthesis, DNA synthesis, mitosis, and cell proliferation [11–13]. On the other hand, Ag is one of the well-known antibacterial agents, which has

*Corresponding authors. Tel.: +60 7 5535961; fax: +60 7 5536222.
E-mail addresses: nidakhann6@gmail.com (N. Iqbal), rafiq@biomedical.utm.my (M.R.A. Kadir), hbr_bala@yahoo.com (H.R. Balaji).

0272-8842/$ - see front matter © 2013 Elsevier Ltd and Techna Group S.r.l. All rights reserved.
http://dx.doi.org/10.1016/j.ceramint.2013.08.125

high thermal stability, exhibits low volatility, and is non-toxic to human cells at low concentrations [14,15].

Most of the studies in the literature have described chemical precipitation, sol–gel, and ion-exchange process as the method of choice for ion doping [16–18]. However, these processes require long preparation hours and expensive chemicals [19–21]. To overcome these limitations microwave refluxing method has been developed [22]. Although previous studies have reported successful individual substitution of several ions such as Ag, Zn, CO_3, and F into HA [23–26], the simultaneous incorporation of Zn and Ag into HA nanoparticles using microwave irradiation has not yet been reported. Therefore, in the present study, we examined the possibility of developing Zn–Ag-doped HA nanoparticles, synthesized using the microwave refluxing method, and determined their benefits in terms of their bioactivity and antibacterial property *in-vitro*.

2. Materials and methods

2.1. Synthesis of Zn–Ag–HA nanoparticles

The reagents used included calcium nitrate tetrahydrate [$Ca(NO_3)_2 \cdot 4H_2O$; Q. Rec™], diammonium hydrogen phosphate [$(NH_4)_2HPO_4$; Q. Rec™], zinc nitrate [$Zn(NO_3)_2$; Emory Laboratory Chemical],Ag nanoparticles (Sigma Aldrich), 30% NH_4OH (Q. Rec™), and deionized water. The wet-chemical precipitation method for the synthesis of Zn–Ag–HA nanoparticles can been expressed as follows:

$$(10-x)Ca^{2+} + xM^{n+} + PO_4^{3-} + 2OH^- Ca_{10-x}M_x(PO_4)_6(OH)_2$$

where $M^{n+}=Ag^+$, Zn^{2+}; $(0 \le x \le 0.8)$.

Zn-substituted HA was synthesized by substituting Ca with Zn (x=0.4 and 0.8), with the atomic ratio of (Ca+Zn)/P set to 1.67. An aqueous solution of Ca and $Zn(NO_3)_2$ was prepared by maintaining a molar ratio of Zn+Ca=1 M (Table 1). Subsequently, 0.6 M $(NH_4)_2HPO_4$ solution was added dropwise to the Ca+Zn solution, and the pH of the mixture was maintained at pH10 by adding NH_4OH. Then, 0.3 wt% Ag nanoparticles was added to the solution and stirred for 30 min. The mixture was refluxed into a modified microwave oven (Samsung; MW71B) at 800 W and 2.45 GHz, and subjected to microwave irradiation under ambient air for 10 min (including 20-s ON and 10-s OFF). The suspension was filtered and washed with deionized water until a pH of 7 was reached. The precipitates were dried at 80 °C in a drying oven for 24 h and heat-treated at 1000 °C (RAMP: 5 °C/min) for 2 h. The Zn–Ag–HA pellets were prepared by pressing 0.4 g of each sample powder in a 12-mm-diameter stainless steel die at 3000 psi for 30 s. Subsequently, the pellets were sintered at 1000 °C for 2 h.

2.2. Sample characterization

Fourier transform infrared (FTIR) Bruker (Optic GmbH) ALPHA-T spectra were recorded over the region of 400–4000 cm^{-1} at a scan rate of 4 cm^{-1}. The X-ray diffraction (XRD) patterns were recorded on Bruker D8 Advance X-ray diffractometer with Cu-Kα radiation. The diffractometer was operated at 40 kV and 40 mA. The data were collected over the 2θ range of 10–60° with a step size of 0.05. The size and morphology of the samples were studied using scanning electron microscopy (SEM; JEOL JSM-6700) and the elemental composition was determined by energy dispersive X-ray spectroscopy (EDX; Hitachi TM3000 tabletop microscope).

2.3. Antibacterial testing

Gram-negative (*E. coli*) and gram-positive (*S. aureus*) bacteria were obtained from the Institute of Medical Research, Kuala Lumpur. For the agar disc diffusion test, solidified nutrient agar medium (Merck) was swabbed with the respective organism (n=4) (1×10^8 CFU/mL). Subsequently, in each plate, four sample discs were fixed at equal distance, and the plates were incubated at 37 °C for 24 h. The antibacterial activity was measured as a zone of inhibition (mm) around the sample discs using a standard steel ruler. The experiment was performed in triplicates.

2.4. In vitro bioactivity testing

Simulated body fluid (SBF) was prepared in the laboratory according to the method developed by Kokubo et al. [26]. The ionic concentration was nearly similar to that of the human blood plasma. The HA pellets of approximately 12-mm diameter and 2.5-mm thickness were immersed in 50 mL of SBF solution maintained at body temperature and incubated for 28 days in a water bath at 37 °C. Subsequently, the pellets were removed from the SBF solution and dried at room temperature and the surface morphologies of HA after immersion was examined by SEM–EDX analysis.

Table 1
Sample ID, corresponding wt (%) and amounts of reagents added.

Sample ID	Added to 100 mL deionized water (g)				Wt%	
	CaN		ZnN		Zn	Ag
	Concentration (M)	Amount (g)	Concentration (M)	Amount (g)		
2.5 Zn–Ag–HA	0.96	45.39	0.04	2.4	2.5	0.3
5 Zn–Ag–HA	0.92	43.79	0.08	4.8	5	0.3

2.5. Cell culture

Normal human osteoblast (NHOst) (CC-2538, USA, Lonza) were used for cell adhesion and MTT assays. The osteoblast cells were cultured in Osteoblast Basal Medium (OBM, 500 mL, Lonza) with OGM Bulletkit (OGM™ single quots®, Lonza) containing 0.5 mL of ascorbic acid, 50 mL of FBS, and 0.5 mL of GA-1000, at 37 °C in a humidified 5% CO_2 incubator.The co-confluent cells were trypsinized and used in all experiments in 12- or 96-well plates.

2.6. Cell adhesion test

All the sample discs were sterilized in a steam autoclave at 120 °C for 30 min and under UV irradiation for 1 h. The discs were placed in each well of the 12-well culture plate and the cells were seeded onto the ceramics discs at a density of 5.4×10^4 cells/sample. The seeded test samples were incubated in a CO_2-incubator under standard culture conditions. The culture medium was aspirated after a 3-day interval and fresh culture medium was carefully added to each well to avoid detachment of cells. After 7 days, the samples were washed thrice with phosphate buffered saline (1 × PBS, pH 7.4), fixed overnight in 4% glutaraldehyde in PBS solution, and post-fixed for 1 h in 1% aqueous osmium tetroxide. After fixation, the sample discs were washed and dehydrated with graded ethanol (30–100% (v/v)). The dehydrated samples were dried in 1:1 and 1: 3 (v/v) alcohol-hexamethyldisi-lazane (HMDS) solution and pure HMDS for 10 min, respectively. The dried samples were sputter-coated and the morphology of the cells was examined under scanning electron microscope.

2.7. Cell viability test

Each sterilized sample disc was incubated in 1500 μL of the medium (Osteoblast Basal Medium) at 37 °C under 5% CO_2 atmosphere. After 3 days, the cultures were centrifuged for 5 min at 220*g* and the supernatant was filtered through a 0.2-μm membrane filter. Normal human osteoblast (NHOst) cells at a density of 1.0×10^4 cells/well were seeded in 96-well plates for 24 h, and subsequently, the culture medium was replaced with fresh medium and incubated for 7 days at 37 °C under 5% CO_2 atmosphere. The conditioned medium was aspirated after 3 days and fresh medium was added to each well. Three replicates were prepared for each group. After the incubation period, the culture medium was aspirated and the samples were washed twice with PBS, and then 100 μL of fresh medium were added to each well. Then, 10 μL of MTT (Invitrogen, M6494) were added to each well and incubated for 4 h. After incubation, the medium was aspired and 100 μL of dimethyl sulfoxide (DMSO; stock solution) were added to each well, and absorbance was measured at 540 nm using automated microplate reader (Tecan, Safire^2). The concentrations were analyzed by SPSS v.16.0 (SPSS Inc., Chicago, IL) using one-way ANOVA followed by post-hoc LSD, with a significant level set at $p < 0.05$.

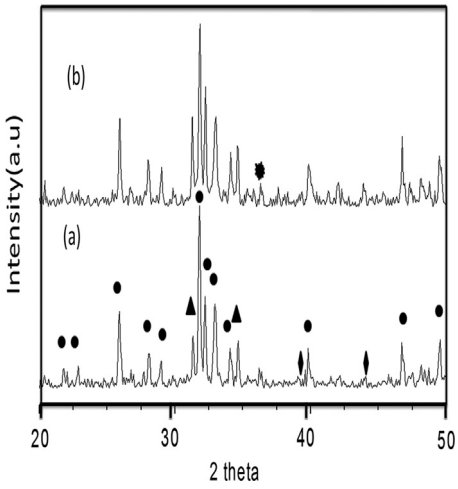

Fig. 1. XRD analysis of Zn–Ag–HA samples heat treated at 1000 °C for 2 h (a) = 2.5 Zn–Ag–HA and (b) = 5 Zn–Ag–HA. Note HA = ●, TCP = ▲, Ag = ◆, Parascholzite = ✹.

3. Results and discussion

The XRD patterns of Zn–Ag–HA samples are shown in Fig. 1. The XRD of 2.5 wt% Zn substitution indicated typical HA peaks at 25.91°, 28.94°, 31.78°, 32.19°, 32.93°, 34.1°, 39.80°, 46.71°, and 49.49°, which were found to be in accordance with the crystalline HA composition [HA, $Ca_5(PO_4)_3(OH)$, JCPDS File # 09-0432]. The peak at 31.71° was identified as Zn-containing β-tricalcium phosphate (β-TCP), which suggested that a small amount of β-TCP might have been formed along with HA due to the addition of Zn. A further increase in the Zn content from 2.5 to 5 wt% resulted in an obvious decrease in the intensity of HA peaks and an increase in the intensity of Zn-TCP. The formation of TCP was due to the difference in the ion sizes of Ca (0.99 Å) and Zn (0.83Å), which led to a distortion of the crystal structure [17,18]. A new peak at 35.6° (Fig. 1) represented $CaZn_2(PO_4)_2 \cdot 2H_2O$ (JCPDS 35-0495), and the minor peaks at 38.1° and 44.4° indicated the presence of metallic Ag (JCPDS 04-783) [27]. The average crystallite size calculated by peak broadening (31.9°) using the Scherrer equation was 63 and 50 nm for 2.5 and 5 wt% Zn–Ag–HA samples, respectively. Thus, the XRD analysis indicated that Zn substitution affected the crystal structure, stability, and thermal decomposition of HA and produced an inhibitory effect on HA formation, which reduced the crystallinity of HA.

The FTIR spectra of Zn–Ag–HA nanoparticles represented characteristic bands of absorbed water, hydroxyl, and phosphate species that corresponded to the HA structure (Fig. 2). The peak at 3571 $cm^{-1}$was attributed to the stretching vibration band (υ_s) of the hydroxyl group of the HA, which indicated the crystalline nature of HA. The band at 1510–1380 cm^{-1} represented asymmetric stretching (υ_3) of the C–O bond of the carbonate group, which revealed that a certain level of carbonate substitution had occurred. Furthermore, Ca (II) and Zn (II) ions in the surface layers of the HA crystals may bind to ambient CO_2. The characteristic stretching vibration (υ_s) of the phosphate group was observed at 1037 and 1096 cm^{-1}. The peak at 951 cm^{-1} corresponded to the

(ν_1) stretching mode of the phosphate group. In addition, the librational mode (υ_L) of the hydroxyl group appeared at 633cm^{-1}, and two sharp peaks at 602 and 569 cm^{-1} were attributed to the bending mode (υ_4) of the O–P–O linkage in the phosphate group of the HA. The peak at 962–1105cm^{-1} was assigned to the P–O stretching vibration of the phosphate group and the weak band of about 470cm^{-1} corresponded to the phosphate bending vibration. A further increase in the Zn content to 5 wt% (for 5 Zn–Ag–HA samples) resulted in an increase in the asymmetric P–O stretching vibration absorption band at 1045 and 1120 cm^{-1}, and a decrease in the O–P–O bending vibration absorption band at 605 cm^{-1}. Moreover, the stretching vibration bands of the absorbed water appeared at 3420 cm^{-1}. As the Zn content increased, a slight shift in the hydroxyl group peak at 3572 cm^{-1} and a considerable broadening of the 700–1700-cm^{-1} phosphate bands were observed. From these observations, it was evident that Zn and Ag had been successfully doped into the HA lattice, and that with increasing Zn content, the crystallinity of the apatite structure decreased.

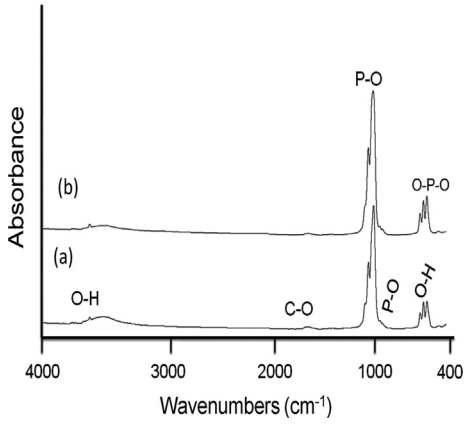

Fig. 2. FTIR analysis of Zn–Ag–HA samples treated at the 1000 °C for 2 h: (a)=2.5 Zn–Ag–HA and (a)=5 Zn–Ag–HA.

Field emission SEM observations of the sample powders revealed that Zn and Ag doping influenced the size of the HA nanoparticles (Fig. 3). The nanoparticles appeared agglomerated and had a round morphology with an average size of 102 nm in diameter. Furthermore, an increase in the Zn ions doped into HA resulted in the fusion of the agglomerated particles. The aggregate, consisting of interconnected elongated spherical-like particles of $\pm$70 nm, exhibited the same degree of porosity ($\pm$63 nm in diameter). The EDX spectra of Zn–Ag–HA composites revealed P, Ca, Ag, and Zn peaks, indicating the presence of these elements in the composites.

Fig. 4 shows the disk diffusion results for the Zn–Ag–HA nanoparticles against the bacteria, *S. aureus* and *E. coli*. The zone of inhibition for the 2.5 Zn–Ag–HA samples against *S. aureus* and *E. coli* was found to be $\pm$0.6 and $\pm$1 mm, respectively. On the other hand, the zone of inhibition for the 5 Zn–Ag–HA samples against *S. aureus* and *E. coli* was comparatively higher at $\pm$0.9 and $\pm$1.0 mm, respectively. In both cases, the Zn–Ag–HA nanoparticles were found to be more effective against gram-negative than gram-positive bacteria. However, no antibacterial action was observed in the HA sample. In contrast to this finding, a previous study

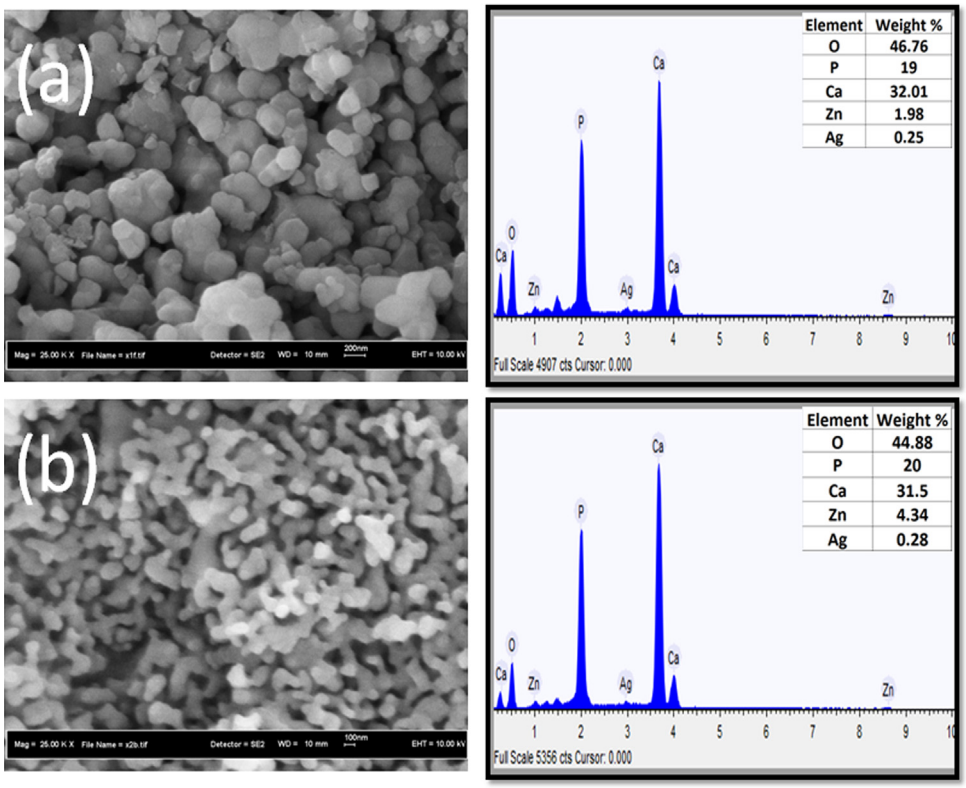

Fig. 3. SEM and EDX analysis of Zn–Ag–HA samples for treated at 1000 °C for 2 h samples: (a)=2.5 Zn-Ag-HA; (b)=5 Zn–Ag–HA.

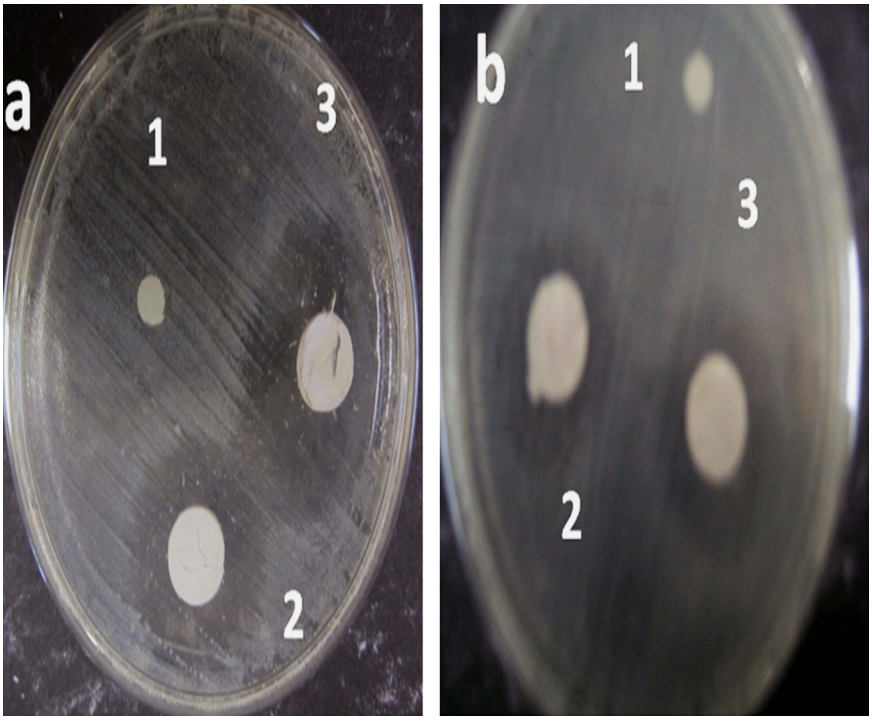

Fig. 4. Antibacterial activity of Zn–Ag–HA samples treated at 1000 °C for 2 h (a); *E. coli*, (b); *S. aureus*, *Note*: (1) HA; (2) 2.5 Zn–Ag–HA; (3) 5 Zn–Ag–HA.

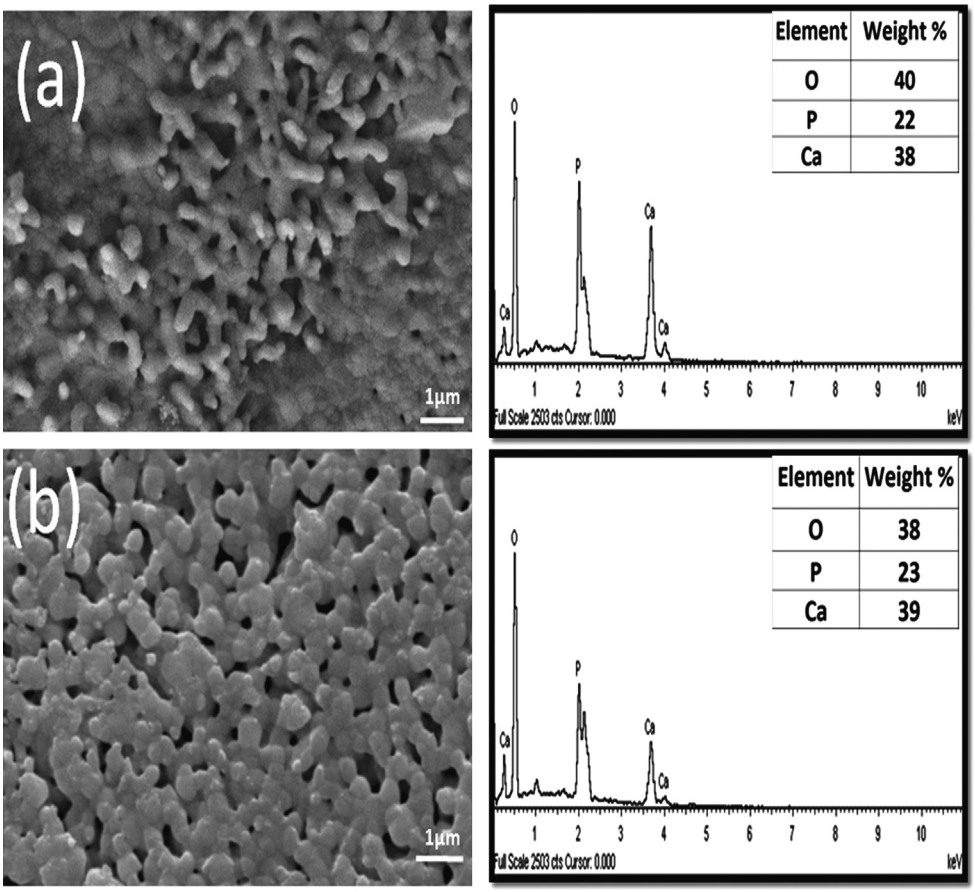

Fig. 5. SEM and EDX analysis of Zn–Ag–HA pallets after immersion in SBF for 28 days: (a)=2.5 Zn–Ag–HA; (b) 5 Zn–Ag–HA.

reported antibacterial activity of HA against *Streptococcus mutants*. The reason for this conflicting result could be due to the antibacterial assay and the type of bacterial strain used [28]. The findings of the present study indicate that the inhibition of bacterial growth around the sample disc may be associated with the presence of Ag and Zn ions doped into HA. These results are in agreement with the observations of previous studies, which demonstrated that Ag or Zn can bind to bacterial DNA, thereby inhibiting replication or inactivation of bacterial protein [17].

Apatite formations in Zn–Ag–HA samples were monitored by SEM and EDS, as shown in Fig. 5. The SEM images indicated that the sample discs were covered with a layer of nanosized crystals with a typical morphology of HA after 28 days of immersion in SBF (Fig. 5a and b). Furthermore, the SEM observations demonstrated that the surfaces of the samples were partially covered by a dense apatite layer with tiny worm-like morphology was observed. The extent of formation of apatite layer increased with the increasing Zn content from 2.5 to 5 wt%, as shown in Fig. 5b. The SEM image of the 5 wt% Zn–Ag–HA sample indicated the presence of circular and elongated agglomerated particles that were linked together with an approximate size of 160 nm in diameter. Therefore, we propose that the presence of high Zn content in the Zn–Ag–HA composites may reduce its crystallinity and promote the formation and growth of apatite material on the surface of the ceramic discs. Furthermore, it is known that an increase in Zn content promotes the precipitation of apatite particles in SBF [18]. The present study demonstrated that even short soaking periods in SBF could induce precipitation of apatite layer on the surface of all the specimens, indicating their high degree of bioactivity. Furthermore, through EDS analysis, the Ca/P ratio was found to be approximately 1.69, confirming the purity of HA (Fig. 5).

Co-substitution of Zn and Ag into HA produced good antibacterial properties and *in-vitro* bioactivity, and the aim of the present study was to use HA nanoparticles with optimal Ag and Zn concentration for hard-tissue applications. To investigate whether normal human osteoblast (NHOst) cells would interact with the Zn–Ag–HA samples, cell adhesion assay was performed. The cell adhesion micrographs (Fig. 6) demonstrated the growth of osteoblast cells on the surfaces of Zn–Ag–HA discs after 7 days of incubation. All the surfaces were able to support cell growth and metabolic activity of (NHOst). SEM images (Fig. 6a and b) revealed that the cells were attached and spread on the Zn–Ag–HA samples as well as the flattened morphology of cells was observed at 7 days after seeding. These results demonstrated that the cosubstitution of Zn and Ag into HA may support the cell growth.

The viability of normal human osteoblast cells (NHOst) on Zn–Ag–HA samples were evaluated using MTT assay. The MTT assay results indicated that the number of metabolically active cells on HA samples increased with the increasing incubation period (Fig. 7). On the other hand, although an increase in the number of osteoblast cells was noted on HA samples with substitutions of Zn and Ag, the cell numbers were not statistically significant from HA cell numbers. These results indicated that Ag and Zn doped into hydroxyapatite had

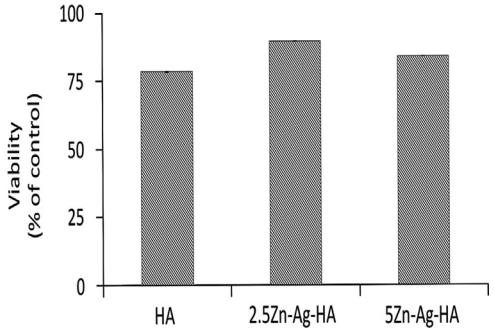

Fig. 7. MTT assay results showing normal human osteoblast (NHOst) cells proliferation on HA, 2.5 Zn–Ag–HA and 5 Zn-Ag-HA samples after 7 days of culture. The data are presented as mean ± SD and values with $p < 0.05$ were considered as statistically non-significant.

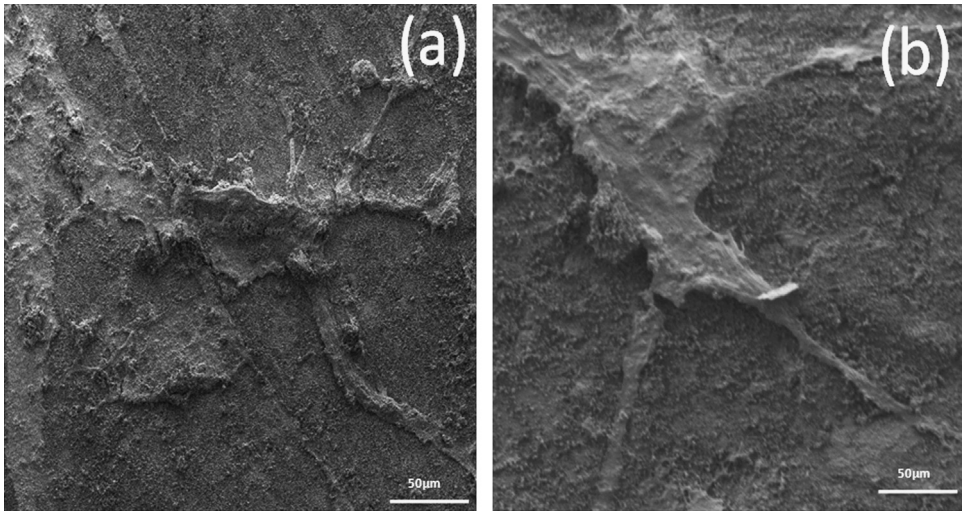

Fig. 6. SEM images (magnification at 1600 ×) of Normal human osteoblast (NHOst) cells adhered to Zn–Ag–HA discs after incubation of 7 days at (a)=2.5 Zn–Ag–HA and (b) 5 Zn–Ag–HA.

no cytotoxic effect on normal human osteoblast cells (NHOst) proliferation. Although it can be seen that the cell proliferation rate of 2.5 Zn–Ag–HA and 5 Zn–Ag–HA samples were 89.9% and 84.2% respectively, after 7 days of incubation statistically it was non-significant. However the reason for the slight decrease in the activity of Zn at higher percentage remains unclear (Fig. 7). These findings demonstrated that the co-substitution of Zn and Ag into HA plays a significant role in promoting cell growth and differentiation. Nevertheless, the mechanism by which Zn and Ag affect the biological response is still unclear and requires further investigation.

4. Conclusion

In the present study, Zn–Ag–HA nanoparticles were successfully synthesized using the microwave refluxing method. The antibacterial properties and bioactivity of the synthesized nanoparticles were found to be superior to those of HA, suggesting that this novel material may be suitable for biomedical applications.

Acknowledgments

The authors would like to thank Nik Ahmad Nazim Nik Malek (Faculty of Biosciences and Medical Engineering, Universiti Teknologi Malaysia (UTM) for his support in antibacterial testing. The authors would like to acknowledge the Institute of Medical Molecular Biotechnology (IMMB), Faculty of Medicine UiTM Campus Sungai Buloh Selangor, Malaysia for providing cell culture facilities. The authors would like to acknowledge the financial support provided by UTM research Grant science funding (Vote: 45027), Ministry of Higher Education (MOHE) and RMC. More than one of the authors of this paper was supported under University of Malaya HIR-MOHE research grant.

References

[1] A.D. Pye, D.E.A. Lockhart, M.P. Dawson, C.A. Murray, A.J. Smith, A review of dental implants and infection, Journal of Hospital Infection 72 (2009) 104–110.
[2] H. Carsenti-Dellamonica, Infections associées aux implants orthopédiques, Antibiotics 10 (2008) 3–15.
[3] W.T.M. Jansen, J.T. van der Bruggen, J. Verhoef, A.C. Fluit, Bacterial resistance: a sensitive issue: complexity of the challenge and containment strategy in Europe, Drug Resistance Updates 9 (2006) 123–133.
[4] L. Crémet, S. Corvec, P. Bémer, L. Bret, C. Lebrun, B. Lesimple, A-F. Miegeville, A. Reynaud, D. Lepelletier, N. Caroff, Orthopaedic-implant infections by *Escherichia coli*: molecular and phenotypic analysis of the causative strains, Journal of Infection 64 (2012) 169–175.
[5] F. Jenny, Fighting bacterial infections—future treatment options, Drug Resistance Updates 14 (2011) 125–139.
[6] H. Oonishi, Orthopaedic applications of hydroxyapatite, Biomaterial 12 (1991) 171–178.
[7] L.L. Hench, Bioceramics—from concept to clinic, Journal of the American Ceramic Society 74 (1991) 1487–1510.
[8] F. Bir, H. Khireddine, A. Touati, D. Sidane, S. Yala, H. Oudadesse, Electrochemical depositions of fluorohydroxyapatite doped by Cu^{2+}, Zn^{2+}, Ag^{+} on stainless steel substrates, Applied Surface Science 258 (2012) 7021–7030.
[9] S. Saidin, P. Chevallier, M. R. Abdul Kadir, H. Hermawan, D. Mantovani, Polydopamine as an intermediate layer for silver and hydroxyapatite immobilisation on metallic biomaterials surface, Materials Science and Engineering C (2013), in Press, http://dx.doi.org/10.1016/j.msec.2013.07.026.
[10] E. Boanini, M. Gazzano, A. Bigi, Ionic substitutions in calcium phosphates synthesized at low temperature, Acta Biomaterialia 6 (2010) 1882–1894.
[11] G.S. Kumar, A. Thamizhavel, Y. Yokogawa, S.N. Kalkura, E.K. Girija, Synthesis characterization and in vitro studies of zinc and carbonate co-substituted nano-hydroxyapatite for biomedical applications, Materials Chemistry and Physics 134 (2012) 1127–1135.
[12] L.C. Ann, S. Mahmud, S.K.M. Bakhori, Electron spectroscopy imaging and surface defect configuration of zinc oxide nanostructures under different annealing ambient, Applied Surface Science 265 (2013) 137–144.
[13] E.S. Thian, T. Konishi, Y. Kawanobe, P.N. Lim, C. Choong, B. Ho, M. Aizawa, Zinc-substituted hydroxyapatite: a biomaterial with enhanced bioactivity and antibacterial properties, Journal of Materials Science: Materials in Medicine 24 (2013) 437–445.
[14] N. Iqbal, M.R. Abdul Kadir, N.A.N. Nik Malek, N. Humaimi Mahmood, M. Raman Murali, T. Kamarul, Rapid microwave assisted synthesis and characterization of nanosized silver-doped hydroxyapatite with antibacterial properties, Materials Letters 89 (2012) 118–122.
[15] V.K. Sharma, R.A. Yngard, Y. Lin, Silver nanoparticles: green synthesis and their antimicrobial activities, Advances in Colloid and Interface Science 145 (2009) 83–96.
[16] V. Stanić, S. Dimitrijević, J. Antić-Stanković, M. Mitrić, B. Jokić, I.B. Plećaš, S. Raičević, Synthesis, characterization and antimicrobial activity of copper and zinc-doped hydroxyapatite nanopowders, Applied Surface Science 256 (2010) 6083–6089.
[17] X. Chen, Q-L. Tang, Y-J. Zhu, C-L. Zhu, X-P. Feng, Synthesis and antibacterial property of zinc loaded hydroxyapatite nanorods, Materials Letters 89 (2012) 233–235.
[18] R-J. Chung, M-F. Hsieh, K-C. Huang, L-H. Perng, F-I. Chou, T-S. Chin, Anti-microbial hydroxyapatite particles synthesized by a sol–gel route, Journal of Sol–Gel Science and Technology 33 (2005) 229–239.
[19] S. Miao, W. Weng, K. Cheng, P. Du, G. Shen, G. Han, S. Zhang, Sol–gel preparation of Zn-doped fluoridated hydroxyapatite films, Surface and Coatings Technology 198 (2005) 223–226.
[20] S. Samani, S.M. Hossainalipour, M. Tamizifar, H.R. Rezaie, In vitro antibacterial evaluation of sol–gel-derived Zn^{+2}, Ag^{+}, and (Zn+Ag)-doped hydroxyapatite coatings against methicillin-resistant Staphylococcus aureus, Journal of Biomedical Materials Research Part A 101 (2013) 222–230.
[21] H. Zreiqat, Y. Ramaswamy, C. Wu, A. Paschalidis, Z. Lu, B. James, O. Birke, M. McDonald, D. Little, C.R. Dunstan, The incorporation of strontium and zinc into a calciumâ€silicon ceramic for bone tissue engineering, Biomaterials 31 (2010) 3175–3184.
[22] N. Iqbal, M.R. Abdul Kadir, N.A.N. Nik Malek, N. Humaimi Mahmood, M. Raman Murali, T. Kamarul, Characterization and antibacterial properties of stable silver substituted hydroxyapatite nanoparticles synthesized through surfactant assisted microwave process, Materials Research Bulletin 48 (2013) 3172–3177.
[23] N.D. Ravi, R. Balu, T.S.Sampath Kumar, Strontium-substituted calcium deficient hydroxyapatite nanoparticles: synthesis characterization and antibacterial properties, Journal of the American Ceramic Society 95 (2009) 2700–2708.
[24] Z. Zou, K. Lin, L. Chen, J. Chang, Ultrafast synthesis and characterization of carbonated hydroxyapatite nanopowders via sonochemistry-assisted microwave process, Ultrasonics Sonochemistry 19 (2012) 1174–1179.
[25] N. Rameshbabu, T.S. Kumar, K. Rao, Synthesis of nanocrystalline fluorinated hydroxyapatite by microwave processing and its invitro dissolution study, Bulletin of Materials Science 29 (2006) 611–615.
[26] T. Kokubo, H. Takadama, How useful is SBF in predicting in vivo bone bioactivity?, Biomaterials 27 (2006) 2907–2915
[27] R. Niranjan, C. Koushik, S. Saravanan, A. Moorthi, M. Vairamani, N. Selvamurugan, A novel injectable temperature-sensitive zinc doped chitosan/β-glycerophosphate hydrogel for bone tissue engineering, International Journal of Biological Macromolecules 54 (2013) 24–29.
[28] O.M. Tin, V. Gopalakrishna, A.R. Samsuddin, K.A. Al-Salihi, O. Shamsuria, Antibacterial property of locally produced hydroxyapatite, Archives of Orofacial Sciences 2 (2007) 41–44.